Research Article | Vol. 12, No. 4 / 1 April 2021 / Biomedical Optics Express 2041
Biomedical Optics EXPRESS

Waveguide-based absorption measurement system for visible wavelength applications

P. NEUTENS,* R. JANSEN, G. WORONOFF, M. RUTOWSKA, N. HOSSEINI, F. BUJA, A. HUMBERT, F. COLLE, T. STAKENBORG, AND W. VAN ROY

Imec, Kapeldreef 75, 3001 Leuven, Belgium
pieter.neutens@imec.be

Abstract: We present a miniaturized waveguide-based absorption measurement system operating at a wavelength of 635 nm, based on a silicon nitride integrated photonic platform, suitable for lab-on-chip applications. We experimentally demonstrate a high correlation between the bulk dye concentration and the measured absorption loss levels in the waveguides. We explain a photonic design process for choosing the ideal waveguide to minimize the coefficient of variation on the analyte concentration. The approach is designed for camera readout, allowing multiple readouts and easy integration for lab-on chip cartridge approach.

1. Introduction

Colorimetry is an absorption-based technique commonly used in clinical chemistry, where the degree of optical transmission directly relates to the amount of analyte present in a solution. Absorbance detection is typically used in e.g. enzymatic assays [1–3], enzyme-linked immunosorbent assays (ELISA) [4,1], etc., where a dye is generated as reporter molecule. Such measurements are generally performed using free-space optics in automated analyzers, plate readers or spectrophotometers [5]. For point-of-care medical testing, there is a significant interest to miniaturize this absorbance detection system and to realize an on-chip alternative [6–8]. Integrated photonics have been shown to be a promising tool to achieve absorbance detection on chip. Previously, silicon photonic waveguide-based absorption sensors have shown great potential for direct gas sensing and glucose sensing in the mid-infrared [9,10].

In this paper, we introduce a photonic waveguide-based absorbance detection system for bulk solutions at visible wavelengths, a choice driven by the dyes commonly used in biological assays. We explain the sensor concept and present a theoretical derivation of the optimal configuration for waveguide-based sensing. A thorough signal to noise analysis is given. In the experimental section, all aspects of data gathering and data analysis are explained. The functioning of the integrated absorbance detection system is verified by performing a dose response measurement with a methylene blue (MB) based dye in buffer for analyte concentrations that are relevant for typical enzymatic assays. The obtained responsivity of the device is compared to the calculation based on the system model.

2. System concept

In photonic waveguide-based absorption measurements, the analyte solution or gas is brought in close proximity to the waveguide, such that it overlaps with the waveguide's evanescent field and leads to an optical absorption dependent on the concentration of the molecule of interest. For label-free approaches [9,10], acquiring the absorption spectrum is essential to differentiate the target analyte from the sample background. In applications relying on the absorption caused by a reporter molecule, absorption at a single wavelength is sufficient. Compared to free space optical instrumentation (an example of ELISA instrumentation can be found in [11]), photonic

#418264 https://doi.org/10.1364/BOE.418264
Journal © 2021 Received 13 Jan 2021; revised 17 Feb 2021; accepted 18 Feb 2021; published 15 Mar 2021

Biomedical Optics EXPRESS

waveguide-based absorption sensors have the ambition to offer the same functionality with a high read-out speed and a comparable or better sensitivity, but with a much smaller footprint, paving the way for point-of-care diagnostic applications [8,12,13]. In addition to the miniaturization, a waveguide-based absorbance measurement system has multiple advantages. While in a plate reader or photospectrometer, the interaction length is limited to the plate well depth or fixed by the cuvette width, the waveguide-based system can be designed with interaction lengths ranging from several microns to tens of centimeters enabling an extremely high dynamic range. This allows the system to measure the absorption losses with a high signal-to-noise ratio for both very weakly and strongly absorbing solutions or gasses with the same measurement system. On-chip absorbance detection systems can be combined with complex microfluidic systems for sample loading, reagent mixing and dilution, thereby requiring only very limited sample volumes. By using photonic waveguides, it is also possible to separate the measurement region from the detector region. Therefore, the waveguide outputs from multiple measurement sites can be routed towards a single detection region, so all waveguide outputs can be imaged in a single frame, allowing the parallel, real-time readout of all measurement sites on the chip without the need of any moving parts. Combining all these advantages can enable a very powerful and compact, real-time, on-chip absorbance detection system.

The waveguide-based absorbance system discussed in this work has been designed with visible wavelengths in mind to match the commonly available dyes for fluorescent and colorimetric assays. Although the concept, the theoretical description and the presented photonics material system in this manuscript are suited for operation over the visible wavelength range, a specific operation wavelength of 635 nm was selected for the experimental demonstrator because of the easy access to very low-cost laser diodes that can be used to create a fully integrated measurement system, and its compatibility with reporter molecules such as Amplite− Red [14] and methylene blue [15–18], as used in a recently reported creatinine assay [19], a marker for kidney function. Silicon nitride (SiN) has been selected as the waveguide material [20,21]. Silicon nitride is compatible with CMOS-based processes for low-cost mass fabrication, possesses a relatively high refractive index (n∼2), does not suffer from two-photon absorption, and has a lower temperature sensitivity than silicon. The colorimetric sensor discussed in this manuscript is fabricated in the imec 200 mm pilot line [20,22] and a detailed overview of the fabrication is discussed in section 4. We use a low-temperature plasma-enhanced chemical vapor deposition (PECVD) process that allows for the integration of SiN photonic circuits onto CMOS wafers in the back-end-of-line. This means that in future designs, the photonics of the waveguide-based system can be integrated onto an imager wafer or other active backbone, allowing the integration of the laser source, photonic chip and detection system in a single device. As the alignment of the imager to the photonics is not critical for this particular application, a non-disposable solution is also feasible, where for example the photonics circuit is fabricated on quartz substrates and positioned on top of a reusable imager chip.

In Fig. 1, a schematic representation of the proposed waveguide-based colorimetry system is shown. The 635 nm measurement light is injected into the chip by coupling the light from a single mode fiber into a single mode waveguide by means of a grating coupler. To route the light towards the detection region, low-loss oxide-cladded single mode rib waveguides are used. By opening the top cladding on top of the waveguide for a specific length and exposing the waveguide to the liquid (the so-called open cladding, green area in Fig. 1), the interaction length where the waveguide senses the absorption of the dyes in the solution can be chosen. In the photonic layout used in this work, the output gratings of all measurement sets are routed towards a centralized detection region. The output signals from this detection region are imaged onto a scientific CMOS camera by means of a standard microscope system, allowing a massive parallel readout of all signals from all measurement sites. The specific implementation of the photonic and fluidic layout will be discussed in section 4.

Biomedical Optics EXPRESS

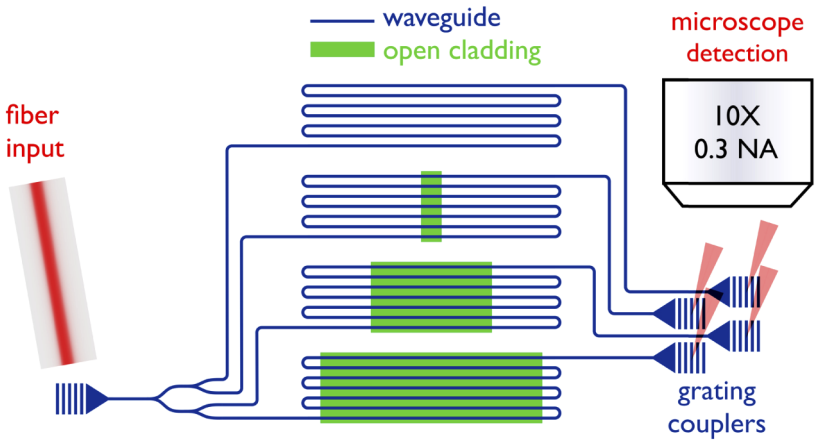

Fig. 1. Schematic overview of the waveguide-based absorbance sensor

3. Theoretical analysis

Choosing the right interaction length with the solution is important to achieve the optimal signal-to-noise ratio for the targeted absorption losses. The optical path length yielding the largest signal-to-noise ratio in absorption measurements has been discussed extensively in literature in the context of spectrophotometry of diluted solutions [23–26]. In that case the absorption by the solute is negligible. The absorption is dominated by the baseline loss of the solvent, and the optimal path length depends only on the absorption coefficient of the solvent (or, translated to a waveguide configuration, the baseline loss of a measurement waveguide). In addition, older treatments usually assume explicitly that the measurement noise is independent of the signal intensity [23–25]. A more recent discussion acknowledges the fact that shot noise (white noise) depends on the signal intensity but did not elaborate the model [26].

The novel analytic model presented below extends the analysis to the case where solute absorption is non-negligible (e.g. a highly absorbing dye) and takes into account the fact that shot noise scales with the signal intensity. We will assume a charge-based detector (such as an imager), where the shot noise on a signal of N collected photons (or electrons) is $\sigma_N = \sqrt{N}$, resulting in a coefficient of variation $CV_N = \sigma_N/N = 1/\sqrt{N}$, or equivalently a signal-to-noise ratio $SNR_N = N/\sigma_N = \sqrt{N}$. However, the results also apply directly to current-based detection, where shot noise on the current is given by the Schottky formula $\sigma_I = \sqrt{2Iq\Delta F}$, with q the elementary charge and ΔF the bandwidth of the detector [27]. Thus $CV_I = \sigma_I/I = \sqrt{2q\Delta F/I} = \sqrt{q/(I\ \Delta t)} = 1/\sqrt{N} = \sigma_N/N = CV_N$, for bandwidth $\Delta F = 1/(2\ \Delta t)$, and with $N = (I\ \Delta t)/q$, where $I\ \Delta t$ is the accumulated charge in the measurement interval Δt. We will also assume waveguide-based measurements, but the result can easily be extended to free space by setting the power fraction in the evanescent field (f) equal to 1, and replacing the attenuation coefficient of the waveguide ($\mu_{10,WG}$) by the free-space attenuation coefficient of the solvent.

The analysis assumes a single waveguide, and measurements with and without the analyte. The Lambert-Beer law in terms of electrons accumulated in the imager for the reference measurement (waveguide in the liquid without solute) reads

$$N_{ref} = N_0\ 10^{-\mu_{10,WG}L} \tag{1}$$

with N_{ref} the number of electrons generated in the detector in the measurement interval Δt (s), L (m) and $\mu_{10,WG}$ (m^{-1}) the length and (decadic) attenuation coefficient of the measurement

Biomedical Optics EXPRESS

section of the waveguide in the liquid but without solute (dye), and N_0 the effective source "power", i.e. the number of electrons that would be generated in the measurement interval Δt for a measurement waveguide length $L = 0$. (This is the number of photons emitted by the light source, reduced by the various losses related to incoupling, routing, splitting, outcoupling, collection, imager quantum efficiency, etc.).

Similarly, the number of electrons N collected in the presence of the solute (or dye) is

$$N = N_0\ 10^{-(\mu_{10,WG}+f\varepsilon_s C_s)L} \tag{2}$$

with ε_s ($M^{-1}\ m^{-1}$) and C_s (M) the (decadic) molar extinction coefficient and molar concentration of the solute, and f the evanescent fraction of the optical power in the liquid. Equation (2) allows us to calculate the expected absorption loss caused by the solute. This loss expressed as optical density (OD) is given by

$$OD = f\varepsilon_s C_s L \tag{3}$$

Considering that our imager is shot noise limited and applying basic error propagation theory, the resulting coefficient of variation (CV) on the solute or dye concentration CV_{C_s} is given by (see Supplement 1 Section S1)

$$CV_{C_s}^2 = \left(\frac{1}{f\varepsilon_s C_s L \ln(10)}\right)^2 \left(\frac{1}{N} + \frac{1}{N_{ref}}\right) \tag{4}$$

Figure 2 shows this coefficient of variation as function of the solute concentration and measurement waveguide length for the system parameters of our practical implementation presented in Section 4. For solute concentrations $C_s \geq 100$ µM the lowest obtainable CV is the same, independent of the concentration, but the waveguide length at which this CV is obtained decreases with increasing concentration. By contrast, for solute concentrations $C_s \leq 10$ µM the lowest obtainable CV decreases (deteriorates) with decreasing concentration, but the optimum waveguide length is independent of the concentration. The cross-over between these two regimes occurs when the losses due to the solute in Eq. (2) are equal to the intrinsic waveguide losses, or thus when $C_s = \mu_{10,WG}/f\varepsilon_s = 22.9$ µM for the parameters used in Section 4.

To find analytical expressions for the waveguide length that gives the lowest CV on the solute concentration, and for the corresponding CV, we take the derivative versus length of Eq. (4) and set this to zero. This gives us the following condition on the length (see Supplement 1 Section S1)

$$2(10^{f\varepsilon_s C_s L} + 1) - L\ln(10)[(\mu_{10,WG} + f\varepsilon_s C_s)10^{f\varepsilon_s C_s L} + \mu_{10,WG}] = 0 \tag{5}$$

The general case has no analytical solution, hence we start with the two limiting cases:

(i) When the waveguide absorption dominates ($\mu_{10,WG} \gg f\varepsilon_s C_s$), setting the solute absorption $f\varepsilon_s C_s = 0$ simplifies Eq. (5) to

$$2(1 + 1) - L\ln(10)[\mu_{10,WG} + \mu_{10,WG}] = 0 \tag{6}$$

and thus

$$L_{opt,WG} = \frac{2}{\ln(10)\mu_{10,WG}} = \frac{0.86859}{\mu_{10,WG}} \tag{7}$$

which is twice the known result for the case where the measurement noise is independent of the path length [24]. This difference can easily be understood: as shot noise decreases with path length (together with the decreasing signal), the shot noise limited situation favors longer path lengths compared to the situation where noise does not decrease with path length.

Biomedical Optics EXPRESS

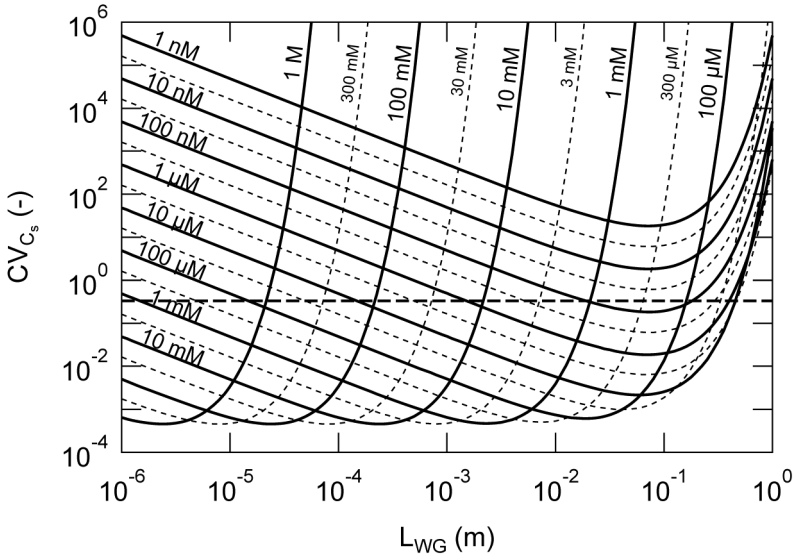

Fig. 2. Coefficient of variation on the measured solute concentration CV_{C_s} as function of the exposed waveguide length L_{WG} for various concentrations according to Eqs. (4), 1 and 2, for the following parameters: baseline loss of the waveguides $\mu_{10,WG}$ = 1.2 dB/cm = 0.12 cm^{-1}, evanescent field fraction f = 0.080, solute molar extinction coefficient ε_s = 50000 $M^{-1}cm^{-1}$, and effective source "power" $N_0 = 10^7$ collected photoelectrons. The dotted horizontal line indicates the common definition of the limit of detection at $CV_{C_s} = 1/3$ or $SNR_{C_s} = 3$.

The minimum CV on the solute concentration is obtained by substituting Eq. (7) into Eqs. (1, 2, 4):

$$N_{ref} = N_0\ 10^{\frac{-2}{\ln(10)}} = N_0/e^2 = 0.13534\ N_0 \tag{8}$$

with e the basis of natural logarithm, not the elementary charge. As waveguide absorption dominates ($\mu_{10,WG} \gg f\varepsilon_s C_s$) or thus $\mu_{10,WG} + f\varepsilon_s C_s \approx \mu_{10,WG}$, Eq. (2) reduces to

$$N \approx N_{ref} \tag{9}$$

and Eq. (4) becomes

$$CV^2_{C_s,\,min} = \left(\frac{1}{f\varepsilon_s C_s L \ln(10)}\right)^2 \frac{2}{N_{ref}} = \left(\frac{\mu_{10,WG}}{2f\varepsilon_s C_s}\right)^2 \frac{2\ e^2}{N_0} = \frac{1}{2\ N_0}\left(\frac{e\ \mu_{10,WG}}{f\varepsilon_s C_s}\right)^2 \tag{10}$$

Hence in the regime of dominating waveguide absorption the minimum CV on the deduced solute concentration $CV_{C_s,\,min}$ decreases with increasing effective source power N_0, but increases (hence, deteriorates) for decreasing solute concentration C_s.

(ii) When absorption by the solute dominates ($f\varepsilon_s C_s \gg \mu_{10,WG}$), setting $\mu_{10,WG} = 0$ reduces Eq. (5) to

$$2(10^{f\varepsilon_s C_s L} + 1) - L\ln(10) f\varepsilon_s C_s 10^{f\varepsilon_s C_s L} = 0 \tag{11}$$

Switching to natural logarithms using $10^x = e^{x\ln(10)}$ and introducing the (napierian) attenuation coefficient of the solute $\mu_s = \ln(10) f\varepsilon_s C_s$ gives the more compact form

$$2(e^{\mu_s L} + 1) - \mu_s L\ e^{\mu_s L} = 0 \tag{12}$$

or

$$e^{\mu_s L}(\mu_s L - 2) = 2 \tag{13}$$

Biomedical Optics EXPRESS

for which Mathematica [28] gives the solution

$$L_{opt,solute} = \frac{2 + W(2/e^2)}{\mu_s} = \frac{2 + W(2/e^2)}{\ln(10) f \varepsilon_s C_s} = \frac{0.963141}{f \varepsilon_s C_s} \tag{14}$$

with $W(x)$ the Lambert-W function [29], and e again the base of the natural logarithm. This scales as the inverse of the solute (or dye) attenuation coefficient, similar to the waveguide (or medium) attenuation coefficient in Eq. (7), but with a slightly larger prefactor. In this regime the count rates N and N_{ref}, and the minimum CV at the optimum waveguide length are independent of the analyte concentration. Substituting Eq. (14) into Eqs. (1), (2) and (4) gives

$$N_{ref} = N_0 \; 10^{-0.963141 \frac{\mu_{10,WG}}{f \varepsilon_s C_s}} \approx N_0 \tag{15}$$

as $\mu_{10,WG} \ll f \varepsilon_s C_s$ or thus $\mu_{10,WG} / f \varepsilon_s C_s \approx 0$, and

$$N \approx N_0 \; 10^{-0.963141 \frac{f \varepsilon_s C_s}{f \varepsilon_s C_s}} = 0.108858 \; N_0 \tag{16}$$

and

$$CV^2_{C_s,\,opt} = \left(\frac{1}{0.963141 \ln(10)} \right)^2 \frac{1}{N_0} \left(\frac{1}{1.08858} + 1 \right) = \frac{2.071122}{N_0} \tag{17}$$

In other words, in this regime the minimum achievable CV (at the optimum waveguide length) depends only on the effective source power N_0.

In the intermediate regime one expects a smooth cross-over between the two extreme regimes that can be approximated by

$$\frac{1}{L_{opt}} = \frac{1}{L_{opt,WG}} + \frac{1}{L_{opt,solute}} \tag{18}$$

or

$$L_{opt} = \left(\frac{\mu_{10,WG}}{0.86859} + \frac{f \varepsilon_s C_s}{0.963141} \right)^{-1} \tag{19}$$

This relationship is illustrated in Fig. 3.

The optimal waveguide lengths are independent of the total power and integration time or bandwidth (as long as read noise and other noise sources remain smaller than the shot noise). However, the magnitude of the measurement error given by Eq. (4) does scale with the total power as $CV_{C_s} \sim 1/\sqrt{N_0}$ (or equivalently $CV_{C_s} \sim 1/\sqrt{I_0}$ in a current-based measurement), through the dependencies of N and N_{ref}, Eqs. (1) and (2).

Finally, we note that the measurement error shown in Fig. 2 has a different behavior for path lengths longer and shorter than the optimal path length. (i) For waveguides longer than the optimal length the error increases exponentially, driven by the exponentially decreasing number of collected photons. (ii) For waveguides shorter than the optimal length, N and N_{ref} approach N_0. Their uncertainties also approach a constant CV_N, $CV_{N_{ref}} = 1/\sqrt{N_0}$, and the increase in CV on the extracted analyte concentration is driven by the linearly decreasing difference between N and N_{ref}.

This implies that it is better to have too short rather than too long path lengths. In practice, a range of interaction lengths can be chosen to make sure the optimal length is present for each possible solute concentration in the assay.

Biomedical Optics EXPRESS

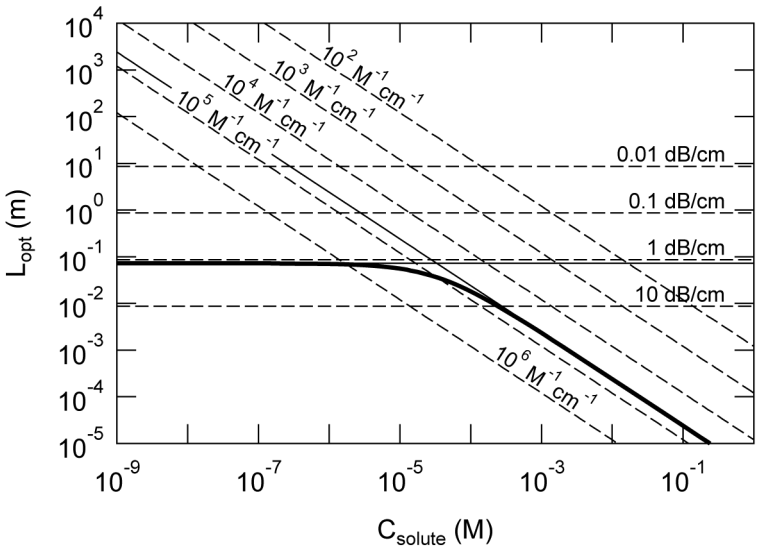

Fig. 3. Optimum waveguide length as function of the solute concentration for the waveguide-limited case (Eq. (7), dashed horizontal lines, labeled with $\mu_{10,WG}$) and the solute-limited case (Eq. (14), tilted lines, labeled with ε_{solute}) with evanescent field fraction $f = 0.080$. Full lines show our specific case with $\mu_{10,WG} = 1.2$ dB/cm and $\varepsilon_{solute} = 50000$ $M^{-1}cm^{-1}$, including the approximate cross-over between both regimes according to Eq. (19).

4. Photonic design and fabrication

In this study, we work with PECVD SiN-based rib waveguides fabricated in a 200 mm CMOS pilot line. The process flow has been described by Subramanian et al. [20]. The PECVD SiO_2 bottom and top cladding have a thickness of 2.3 and 1.0 µm, respectively. The thickness of the PECVD SiN waveguides is 220 nm. Open-cladded waveguides are manufactured by opening the top oxide cladding above the SiN waveguide.

In the next paragraph, the main aspects of the photonics design are discussed. For detailed information on the individual photonic components, we refer the reader to section S3 of the Supplement 1. We inject the transverse-electric (TE) mode in the waveguide and only use the TE mode for sensing. In principle TM operation gives better sensing performance due to the higher field concentrations in the analyte and the lower effect of side wall roughness on the waveguide propagation loss. However, in practice, the TE mode is preferred due to a much lower insertion loss for the grating couplers compatible with the used fabrication technology. At a wavelength of 635 nm, the measured refractive index of the used SiN and SiO_2 is 1.89 and 1.46 respectively. In order to guarantee single mode operation, a waveguide thickness of 220 nm is chosen, with widths of 340 in the oxide-cladded and 480 nm in the open-cladded areas. The transition between the two waveguide widths is realized with a 50 µm long adiabatic taper under oxide cladding, and the open-cladding region starts 50 µm beyond the taper. Figure 4 shows the power fraction in the solution for a rib waveguide as function of the waveguide width, simulated with the mode solver of Lumerical [30]. From this graph, it is clear that reducing the width leads to more field in the fluid, and therefore a shorter interaction length needed to achieve the same absorption. However, a reduced width also leads to increased losses [20]. A width of 480 nm was chosen as a good compromise to achieve a reasonable power fraction in the solute while maintaining a low inherent waveguide propagation loss due to sidewall roughness. A cleaning protocol developed to achieve a clean and low-loss surface for the SiN waveguides was applied and can be found in

Biomedical Optics EXPRESS

[22]. This results in photonic waveguides with a propagation loss of 1.2 dB/cm in water and a power fraction of 8%.

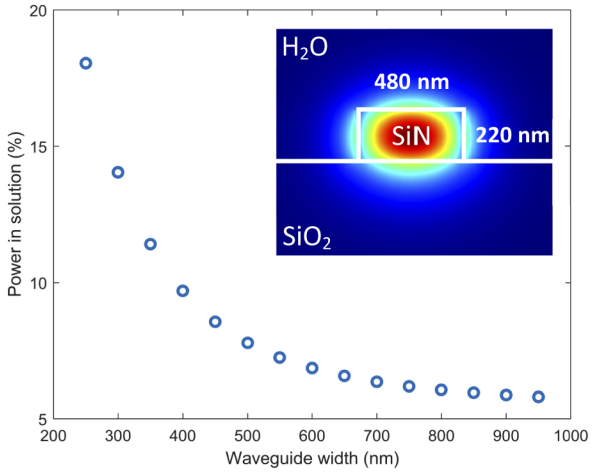

Fig. 4. Simulated power fraction in the solution (water) versus the waveguide width for a 220 nm thick SiN waveguide in water for a wavelength of 635 nm. The inset shows the electric field profile of the first order TE mode for a width of 480 nm.

Given the propagation loss of 1.2 dB/cm, Fig. 3 yields a maximum useful waveguide interaction length of about 10 cm for low-concentration analytes. In practice we use a maximum interaction length of 4.68 cm due to space constraints. However, Fig. 2 tells us that a slightly shorter waveguide only leads to a small reduction in signal-to-noise ratio. Also, shorter waveguides are included to cover a large dynamic range of absorption losses, in the case of a high concentration of analytes or surface-immobilized dyes. A single absorption measurement site can be seen in Fig. 5(c). Waveguides are depicted in blue and the open cladding regions in green. Each measurement site contains 14 different waveguides with interaction lengths between 0.007 and 4.68 cm. The SiN waveguides are fabricated by etching a 4.5 µm slot in the SiN layer around the waveguide core. This slot width of 4.5 µm and a 13 µm distance between neighboring waveguides is implemented to ensure no coupling occurs between the waveguides. The waveguides are folded 6 times in a meandering fashion to fit all waveguides onto a colorimetric chip with a compact footprint. This results in 14 oxide-water cladding transitions. The transition between the oxide and water cladding causes a transition loss due to the mode mismatch and scattering at the interface. This loss factor has been measured on dedicated test structures containing waveguides with different numbers of oxide-water cladding transitions and contributes to 0.09 dB per transition, or 1.26 dB for the full waveguide. Circular bends with a bend radius of 30 µm are implemented, having a bend loss of 0.04 dB per 90-degree bend as measured on dedicated test structures, resulting in a 1.04 dB total bend loss for the waveguides in the set. The oxide cladding is only opened in the straight section. The loss in the bend sections and the scattering loss occurring at the interface between the cladded and open-cladded regions can be compensated for as the number of bends and interfaces are exactly the same for all waveguides. In each site, two more waveguides are present, adding up to a total of 16 waveguides per site. One completely oxide-cladded waveguide is present, used to measure the loss of the oxide-cladded routing waveguides based on the difference in transmission between the 4 measurement sites with different overall routing length. The layout of the full colorimetric chip can be seen in Fig. 5(a). Each chip contains 2 groups of 4 measurement sites that are rotated 180 degrees around the center of the chip. One group of 4 measurement sites has a single input grating coupler and

Biomedical Optics EXPRESS

64 output grating couplers. In this way, 64 output couplers can be measured simultaneously by the microscope setup, allowing us to monitor the propagation loss of 4 waveguide sets in real-time. To equally divide the optical power from the input to the 64 different waveguides, we use a balanced fractal tree with 6 levels of symmetric multimode interference (MMI) splitters. The outputs of each measurement site allow us to determine the absorption loss caused by the solution, while the difference in routing waveguide length between the 4 different sites allows us to easily calculate the oxide cladded waveguide propagation loss as a reference measurement.

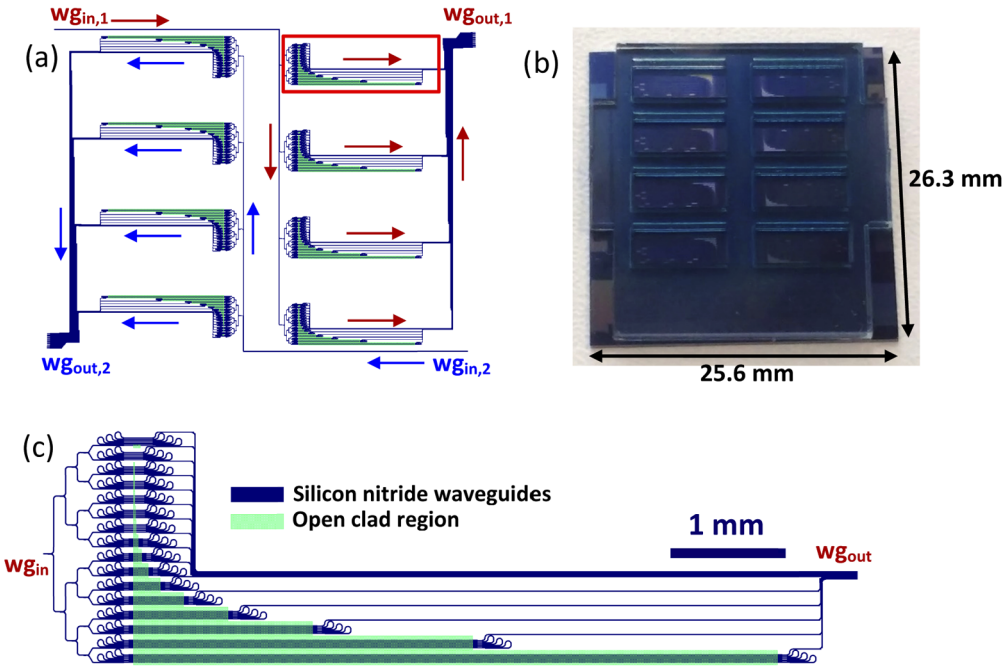

Fig. 5. (a) Layout of the full colorimetry photonic chip, consisting out of 8 sets of waveguides. A single waveguide set consisting of 16 measurement waveguides is marked by the red rectangle. Light propagation in the two sets is shown by the red and blue arrows. (b) Picture of the full colorimetric chip with the PMDS fluidic gasket attached. Cuts in the gasket are foreseen at the position of the input and output waveguides. (c) Zoom in on a single waveguide set consisting out of 16 waveguides with different air cladding lengths.

Coupling light in and from the chip is realized by standard grating couplers combined with a linear taper. The 6 µm wide gratings have a full 220 nm deep etch, a constant grating pitch of 460 nm and a gap of 255 nm, yielding an insertion loss of 8.7 dB at an optimum fiber angle of 10 degrees and the operating wavelength of 635 nm. Coupling in light is done by fiber coupling to a single input grating coupler, while the parallel detection of all output grating coupler intensities is realized with a microscope and a scientific CMOS imager. The grating coupler emission is centered at an angle of 10 degrees with respect to the vertical. A custom-made silicone gasket is attached to the chip in order to create a fluidic well on top of each measurement site. To clean the silicone gasket, it is submerged in an ethanol:methanol (95:5) mixture in an ultrasonic bath for 5 minutes. Afterwards the gasket is kept in DI water for an hour. A picture of the full chip with silicone gasket attached is shown in Fig. 5(b). A description of the design and layout of the photonic chip can be found in section S2 of the Supplement 1 and a more elaborate description of all used photonic components is given in section S3 of the Supplement 1. In dedicated designs, the number of wells that can be read out in parallel can be increased significantly, and the number

Biomedical Optics EXPRESS

of waveguides needed for a specific application can be reduced, decreasing the footprint of the device.

5. Experimental results

5.1. Experimental setup

To measure the absorption loss caused by the analyte, we use a custom-built microscope setup. The setup is built around the Hamamatsu ORCA Flash 4.0 scientific CMOS camera (full well capacity: 30000e-, read noise: ~1.5e-, dark current: 0.06 e-/well/s at −10 °C [31]). The photonic chip is mounted on a vacuum sample holder that is fixed on top of an automated 3D translation stage which provides the positioning of the output grating couplers inside the microscope field of view. On top of the 3D translation stage, an automated fiber positioner is mounted, providing alignment of the input fiber with respect to the input grating coupler. The laser source is a fiber coupled Bluesky research FTEC 2635-V50PA0. A fiber U-bench with laser cleanup filter and polarization paddles are used to optimize the spectrum and the polarization of the measurement light. The power output from the fiber can both be controlled electronically as with ND filters in the U-bench. The microscope is fitted with a Nikon N10X-PF objective with a NA of 0.3, allowing both a large field of view and a collection angle sufficient to capture the light emission at 10 degrees from the output grating couplers. This allows us to measure the power output from 64 output grating couplers in parallel (4 sets of 16 waveguides, see Fig. 5(a)). The entire setup is controlled via a Labview program. Analysis of the frames was performed in real-time by means of a Matlab analysis script.

5.2. Propagation loss measurements

The propagation loss of each measurement site is determined by the cutback method, for which we use the power output values of 14 of the 16 different waveguide lengths. The top two waveguides are not used for the propagation loss calculation in solution, as they share a different number of solution-oxide crossings than the other waveguides, but are used to determine the propagation loss of the oxide cladded routing sections. The 14 waveguides used for the propagation loss calculation have interaction lengths between 0.007 and 4.67845 cm. When performing a measurement, for each time point we take 22 frames with integration times between 1.5 and 7481 ms (in steps of 1.5x) in order to have the highest possible dynamic range for the measurement, so both very high and very low losses can be measured with high accuracy. 5 sets of background frames were taken with the same integration times before the start of the measurements. In the analysis software, each output grating coupler is selected by a 41×41 pixel region of interest (ROI). For each ROI, we select the frame with the longest integration time without any saturated pixels, subtract the corresponding ROI from the averaged background frame with the same integration time, and divide it by the integration time to convert intensity to flux. The values of all pixels in the resulting normalized 41×41 pixel frame are summed for each output grating coupler. These values are converted to a dB scale. The propagation loss of the oxide cladded routing waveguides is then automatically calculated using the waveguides without open cladding of the 4 measurement sites. This value is used for correcting for differences in routing waveguide lengths between the 14 different waveguides within each set. The results are fitted linearly vs the open clad length to extract the propagation loss.

5.3. Methylene blue (MB) dose response curve

As a proof-of-principle experiment, we use the waveguide-based absorbance sensor to measure a dilution series of methylene blue (MB) in Tris (tris(hydroxymethyl)aminomethane) buffer (Tris 100 mM, pH 7.4). The measured molar extinction coefficient of methylene blue in tris buffer is shown in Fig. 6(a), with the red line indicating the measurement wavelength. At the wavelength of

Biomedical Optics EXPRESS

635 nm, the molar extinction ratio has a value of 5.3×10^4 $M^{-1}cm^{-1}$. The chosen concentrations of 0, 20, 40 and 80 µM are based on the expected range for the creatinine (kidney marker) enzymatic assay developed by Jimenez Valencia et al. [19]. Based on the reference range in the overall population, the background creatine concentration, spiking in of additional creatinine concentrations in the calibrator samples and a 5 to 6-fold dilution from the patient sample to the final assay mix, a final reporter dye concentration in the range of 0–80 µM is expected. The methylene blue dose-response measurement will allow us to assess if the propagation loss caused by the absorption of methylene blue corresponds with the calculated theoretical loss as derived in section 3 of the paper.

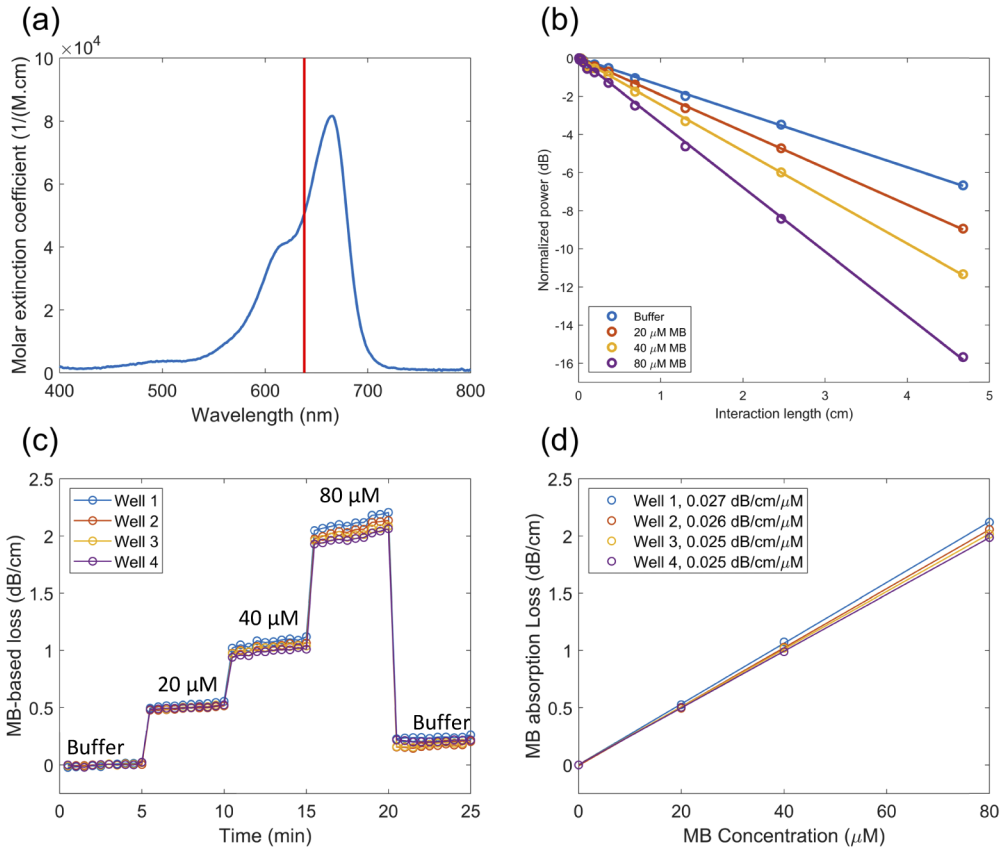

Fig. 6. (a) Measured molar extinction coefficient of MB. The red line indicates the measurement wavelength. (b) Plot of all waveguide output power values of a single measurement set for 4 different MB concentrations. (c) Measured MB-induced waveguide propagation loss for four different MB concentrations. (d) MB dose response curve.

A plot of all output coupler powers of a single measurement site for different concentrations of methylene blue can be seen in Fig. 6(b), together with the fit to calculate the propagation loss. The powers are normalized to the output power of the shortest interaction length (70 µm). According to the Lambert-Beer law, an exponential decay is observed with a larger decay constant for higher MB concentrations. The experiment is run on 4 waveguide sets on the chip simultaneously to look at the variation between different measurement sites. The calculated waveguide propagation loss caused by MB as a function of time can be seen in Fig. 6(c). To start, each well is filled with 75 µL of Tris buffer and a 5-minute measurement is taken as the baseline absorption loss. Then the solution in each well is sequentially replaced by the MB solutions with different concentrations.

Biomedical Optics EXPRESS

For each concentration, 10 measurements are taken over a time span of 5 minutes. For each measurement point, the propagation loss is fitted (as is shown in Fig. 6(b)) and the absorption loss caused by MB is calculated for each well. When switching the MB solution in the fluidic well, 60 µL is pipetted out of the well and replaced by 60 µL of the new solution, followed by a short mixing step. This process is repeated 3 times and was chosen to make sure the waveguide surface wouldn't dry in order to avoid surface sticking of MB. This process leaves 0.8% of the old liquid in the fluidic well, leading to a very small error in the MB concentration. A clear increase of the absorption loss proportional to the MB concentration is observed. After the dose response measurement, the sample is cleaned in DI water and another buffer measurement is run. We observe an increase of the buffer level of 0.2 dB/cm compared to the initial buffer measurement, suggesting we suffer from a small amount of unwanted non-specific binding or sedimentation of MB onto the waveguide surface. This effect can also be seen as an increase of the absorption loss as a function of time for the higher concentrations. To use MB as a substrate for an enzymatic assay, further assay development needs to be done to prevent non-specific binding to the surface.

The dose response curve is shown in Fig. 6(d) for all 4 measurement sites. The average of the 10 absorption loss datapoints for each MB concentration is plotted as a function of the MB concentration. We find experimental sensitivities between 0.025 and 0.027 dB/cm/µM. This is in reasonable agreement with the expected loss value of 0.043 dB/cm/µM predicted by Eq. (3), using the measured MB molar extinction coefficient of $5.3.10^4$ $M^{-1}cm^{-1}$ at 635 nm and a power fraction in the waveguide evanescent field of 0.08. A possible reason for the small discrepancy could be processing variations, mainly width and thickness variations of the waveguide and individual scattering defects in the waveguides, which may also account for the small variations between the different wells (measurement sites) seen in the measurements. Although the repeatability of both the measurement system and the chip leave some room for further improvements, the dose response curves demonstrate that the waveguide-based absorption measurement is capable of detecting methylene blue or other substances absorbing at a wavelength of 635 nm in a relevant range of concentrations for running an enzymatic assay.

6. Conclusions

We presented a waveguide-based absorbance sensor for visible wavelengths based on a silicon nitride photonics platform. A theoretical derivation of the optimum sensor length has been given, and the optimum sensor length was calculated as a function of solute concentration. The coefficient of variation on the measured concentration as function of the waveguide length was calculated for various concentrations in order to assess how the signal-to-noise ratio varies when moving away from the optimum sensor length. Based on the theoretical derivation, a sensor chip has been designed and fabricated. We measured the absorption caused by a dilution series of methylene blue in Tris buffer as a proof-of-principle experiment. The methylene blue concentrations were chosen so they covered a relevant range to be used in enzymatic assays. The dose response curve produced by the waveguide-based sensor yielded a sensitivity in close agreement to the theoretical value. The sensor's sensitivity and signal-to-noise ratio are proven to be sufficient to be used as a small-footprint alternative for commercial plate readers to perform absorption based biological assays. The used PECVD silicon nitride platform allows further integration of the photonic circuitry on CMOS imagers and hybrid integration of a laser source, paving the way for a fully integrated absorbance sensor for point-of-care applications.

Funding. miDIAGNOSTICS.

Acknowledgements. The authors thank William Clarke, Angela Jimenez Valencia, Lindsay Kryszak and Matthew Olson (Johns Hopkins University School of Medicine, Baltimore) for discussions on the application cases for the absorbance-based measurement system.

Disclosures. The authors declare that there are no conflicts of interest related to this article.

Biomedical Optics EXPRESS

Supplemental document. See Supplement 1 for supporting content.

References

1. R. Eisenthal and M. J. Danson, *Enzyme Assays: A Practical Approach* (Oxford University Press, 2002).
2. J. P. Goddard and J. L. Reymond, "Enzyme assays for high-throughput screening," Curr. Opin. Biotechnol. **15**(4), 314–322 (2004).
3. W. Van Roy, G. Woronoff, A. M. Jimenez Valencia, T. Stakenborg, and W. A. Clarke, "Analytical description of the lag phase in coupled-enzyme substrate assays," Biochem. Eng. J. **161**, 107699 (2020).
4. E. Engvall and P. Perlmann, "Enzyme-linked immunosorbent assay (ELISA) quantitative assay on immunoglobulin G," Immunochemistry **8**(9), 871–874 (1971).
5. J. A. Lott and D. A. Nealon, *Methods of Biochemical Analysis* (John Wiley & Sons, 1993).
6. A. Larsson, R. Greig-Pylypczuk, and A. Huisman, "The state of point-of-care testing: a european perspective," Upsala J. Med. Sci. **120**(1), 1–10 (2015).
7. R. Daw and J. Finkelstein, "Lab on a chip," Nature **442**(7101), 367 (2006).
8. G. L. Duveneck, A. P. Abel, M. A. Bopp, G. M. Kresbach, and M. Ehrat, "Planar waveguides for ultra-high sensitivity of the analysis of nucleic acids," Anal. Chim. Acta **469**(1), 49–61 (2002).
9. L. Tombez, E. J. Zhang, J. S. Orcutt, S. Kamlapurkar, and W. M. J. Green, "Methane absorption spectroscopy on a silicon photonic chip," Optica **4**(11), 1322–1325 (2017).
10. E. Ryckeboer, R. Bockstaele, M. Vanslembrouck, and R. Baets, "Glucose sensing by waveguide-based absorption spectroscopy on a silicon chip," Biomed. Opt. Express **5**(5), 1636–1648 (2014).
11. S. Aydin, "A short history, principles, and types of ELISA, and our laboratory experience with peptide/protein analyses using ELISA," Peptides **72**, 4–15 (2015).
12. C. Monat, P. Domachuk, and B. Eggleton, "Integrated optofluidics: A new river of light," Nat. Photonics **1**(2), 106–114 (2007).
13. M. Seidel and R. Niessner, "Automated analytical microarrays: a critical review," Anal. Bioanal. Chem. **391**(5), 1521–1544 (2008).
14. AAT Bioquest, https://www.aatbio.com.
15. N. Ohishi, H. Ohkawa, A. Miike, T. Tatano, and K. Yagi, "A new assay method for lipid peroxides using a methylene blue derivative," Biochem. Int. **10**(2), 205–211 (1985).
16. K. Yagi, K. Kiuchi, Y. Saito, A. Miike, N. Kayahara, T. Tatano, and N. Ohishi, "Use of a new methylene blue derivative for determination of lipid peroxides in foods," Biochem. Int. **12**(2), 367–371 (1986).
17. K. Yagi, S. Komura, N. Kayahara, T. Tatano, and N. Ohishi, "A simple assay for lipid hydroperoxides in serum or plasma," J. Clin. Biochem. Nutr. **20**(3), 181–193 (1996).
18. T. Okumiya, Y. Jiao, S. Toshiji, A. Miike, K. Park, T. Kageoka, and M. Sasaki, "Sensitive enzymatic assay for erythrocyte creatine with production of methylene blue," Clin. Chem. **44**(7), 1489–1496 (1998).
19. A. M. Jimenez Valencia, L. A. Kryszak, J. Goheen, W. Van Roy, G. Woronoff, E. Mathieu, H. Gudjonsdottir, T. Stakenborg, and W. A. Clarke, "Rapid quantification of plasma creatinine using a novel kinetic enzymatic assay," J. Appl. Lab. Med. (2020).
20. A. Z. Subramanian, P. Neutens, A. Dhakal, R. Jansen, T. Claes, X. Rottenberg, F. Peyskens, S. H. P. Selvaraja, B. Du bois, K. Leyssens, S. Severi, P. Deshpande, R. Baets, and P. Van Dorpe, "Low-loss singlemode PECVD silicon nitride photonic wire waveguides for 532–900 nm wavelength window fabricated within a CMOS pilot line," IEEE Photonics J. **5**(6), 2202809 (2013).
21. D. J. Blumenthal, R. Heideman, D. Geuzebroek, A. Leinse, and C. Roeloffzen, "Silicon Nitride in Silicon Photonics," Proc. IEEE **106**(12), 2209–2231 (2018).
22. P. Neutens, M. Rutowska, W. Van Roy, R. Jansen, F. Buja, and P. Van Dorpe, "Mitigation of UV-Induced Propagation Loss in PECVD Silicon Nitride Photonic Waveguides," ACS Photonics **5**(6), 2145–2150 (2018).
23. R. Cole, "Optimum optical density in spectrophotometry," J. Opt. Soc. Am. **41**(1), 38–40 (1951).
24. P. S. Jensen and J. Bak, "Near-infrared transmission spectroscopy of aqueous solutions: influence of optical pathlength on signal-to-noise ratio," Appl. Spectrosc. **56**(12), 1600–1606 (2002).
25. H. L. Mark and P. Griffiths, "Analysis of noise in Fourier transform infrared spectra," Appl. Spectrosc. **56**(5), 633–639 (2002).
26. K. B. Mogensen and J. P. Kutter, "Optical detection in microfluidic systems," Electrophoresis **30**(S1), S92–S100 (2009).
27. W. Schottky, "Über spontane Stromschwankungen in verschiedenen Elektrizitätsleitern," Ann. Phys. **362**(23), 541–567 (1918).
28. Mathematica, https://www.wolfram.com/mathematica.
29. Wolfram Mathworld, http://mathworld.wolfram.com/LambertW-Function.html.
30. Lumerical, http://www.lumerical.com.
31. Hamamatsu, http://www.hamamatsu.com.